Title

Plasticity of Recurrent L2/3 Inhibition and Gamma Oscillations by Whisker Experience

Journal

Neuron, 80(1)

ISSN

0896-6273

Authors

Shao, Yu R
Isett, Brian R
Miyashita, Toshio
et al.

Publication Date

2013-10-01

DOI

10.1016/j.neuron.2013.07.026

Peer reviewed

Neuron
Article

Plasticity of Recurrent L2/3 Inhibition and Gamma Oscillations by Whisker Experience

Yu R. Shao,[1,2] Brian R. Isett,[1,2] Toshio Miyashita,[1,2,4] Jason Chung,[1,2,5] Olivia Pourzia,[1,2] Robert J. Gasperini,[3] and Daniel E. Feldman[1,2,*]
[1]Department of Molecular and Cellular Biology
[2]Helen Wills Neuroscience Institute
University of California Berkeley, Berkeley, CA 94720, USA
[3]Menzies Research Institute, University of Tasmania, Tasmania, 7001, Australia
[4]Present Address: Division of Developmental Neurophysiology, National Institute for Physiological Sciences, National Institutes of Natural Sciences, Okazaki, Aichi 444-8787, Japan
[5]Present Address: Medical Scientist Training Program, UCSF, San Francisco, CA 94143, USA
*Correspondence: dfeldman@berkeley.edu
http://dx.doi.org/10.1016/j.neuron.2013.07.026

SUMMARY

Local recurrent networks in neocortex are critical nodes for sensory processing, but their regulation by experience is much less understood than for long-distance (translaminar or cross-columnar) projections. We studied local L2/3 recurrent networks in rat somatosensory cortex during deprivation-induced whisker map plasticity, by expressing channelrhodopsin-2 (ChR2) in L2/3 pyramidal cells and measuring light-evoked synaptic currents in ex vivo S1 slices. In columns with intact whiskers, brief light impulses evoked recurrent excitation and supralinear inhibition. Deprived columns showed modestly reduced excitation and profoundly reduced inhibition, providing a circuit locus for disinhibition of whisker-evoked responses observed in L2/3 in vivo. Slower light ramps elicited sustained gamma frequency oscillations, which were nearly abolished in deprived columns. Reduction in gamma power was also observed in spontaneous LFP oscillations in L2/3 of deprived columns in vivo. Thus, L2/3 recurrent networks are a powerful site for homeostatic modulation of excitation-inhibition balance and regulation of gamma oscillations.

INTRODUCTION

Experience regulates multiple components of cortical microcircuits to mediate sensory map plasticity. Plasticity in long-range excitatory circuits (thalamocortical, translaminar and cross-columnar) is well characterized and often follows Hebbian rules in which deprived inputs weaken or lose synapses, and spared inputs strengthen or add synapses (e.g., Antonini and Stryker, 1993; Allen et al., 2003; Trachtenberg and Stryker 2001; Broser et al., 2008; Yamahachi et al., 2009). In contrast, the contribution of local recurrent circuits to cortical plasticity is much less understood. Local recurrent circuits help generate sensory tuning (Schummers et al., 2002) and include both recurrent excitation and inhibition whose ratio regulates sensory gain and information flow (Adesnik and Scanziani, 2010; Atallah et al., 2012). Recurrent inhibition from fast-spiking (FS) interneurons generates gamma oscillations (30–90 Hz), which synchronize local spikes and may promote formation of cell assemblies and information transfer to higher areas (Fries, 2009; Buzsáki and Wang, 2012). Thus, local recurrent circuits may be a powerful nexus for regulation of cortical information processing. Experience can alter some components of recurrent circuits (Maffei et al., 2004, 2006; Cheetham et al., 2007; Maffei and Turrigiano 2008), but the net functional effect, and whether this plasticity is functionally distinct from plasticity in long-range circuits, is not known. Local circuits are intermixed with long-range axons and therefore cannot be studied selectively using classical extracellular stimulation. Here, we use optogenetics to selectively activate local recurrent circuits and measure the functional changes that accompany map plasticity.

We focus on L2/3 of somatosensory cortex, which is a major site of receptive field reorganization during whisker map plasticity (Glazewski and Fox, 1996). Rats have five rows of whiskers, termed A–E, represented in S1 by an isomorphic map of cortical columns. Thalamocortical input arrives principally in L4, which projects to L2/3. L2/3 pyramidal (PYR) cells make glutamatergic synapses on nearby PYR cells (recurrent excitation) and on L2/3 and L5 interneurons that inhibit L2/3 PYR cells (recurrent inhibition) (Reyes et al., 1998; Kapfer et al., 2007; Lefort et al., 2009). Plucking the D row of whiskers in juvenile animals causes whisker map plasticity in which spiking responses to deprived whiskers are depressed in L2/3 of deprived columns, while L4 remains relatively unaffected (Drew and Feldman, 2009; Jacob et al., 2012). Major loci of this Hebbian weakening are the L4→L2/3 feedforward projection (Allen et al., 2003; Shepherd et al., 2003; Bender et al., 2006) and L2/3 cross-columnar projections (Broser et al., 2008). How deprivation alters L2/3 recurrent circuit function is unknown.

We hypothesized that local recurrent L2/3 circuits are a major site of compensatory (homeostatic) plasticity that stabilizes, rather than weakens, cortical firing during whisker deprivation. This could occur if deprivation preferentially weakened recurrent inhibition relative to excitation. Such disinhibition could explain

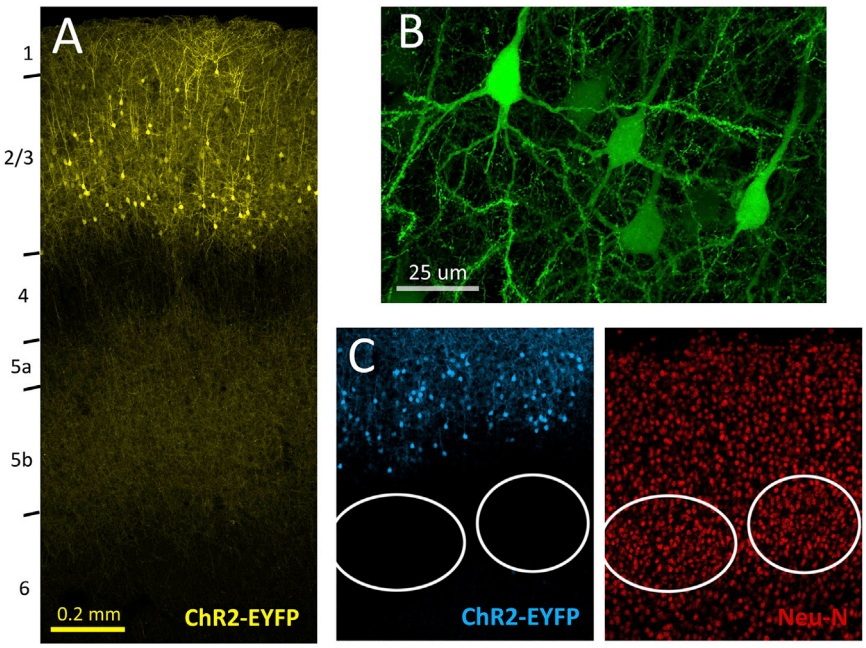

Figure 1. ChR2 Expression in L2/3 Pyramidal Neurons following In Utero Electroporation

(A) ChR2-EYFP expression in S1 of a P24 rat, showing somatodendritic labeling in L2/3 pyramidal cells and axonal branches in L2/3 and L5. Laminar boundaries were determined from DAPI staining (data not shown).

(B) Labeled pyramidal cells.

(C) Double immunostaining for ChR2-EYFP and the neuronal marker Neu-N. Ovals are L4 barrels.

the reduction in whisker-evoked inhibition observed in L2/3 pyramidal cells in vivo (Gambino and Holtmaat, 2012). Homeostasis is critical for cortical function but remains much less understood than Hebbian plasticity (Turrigiano, 2012), and identification of L2/3 recurrent circuits as a major site for homeostatic plasticity would be novel. If a preferential loss of inhibition occurs within recurrent L2/3 circuits, it may also have an effect on gamma oscillations. Plasticity of gamma oscillations is a predicted effect of synaptic plasticity in cortical fast-spiking networks (Paik and Glaser, 2010) but has not yet been directly observed.

RESULTS

We studied functional activation of L2/3 recurrent circuits by optogenetic activation of L2/3 pyramidal cells using channelrhodopsin-2 (ChR2). (L2/3 recurrent circuits cannot be selectively activated by extracellular electrical stimulation because of intermixed feedforward and cross-columnar axons.) ChR2(H134R)-EYFP fusion protein (Nagel et al., 2005), cytosolic GFP, and the red fluorescent protein DsRed were coexpressed (using three independent plasmids) in L2/3 pyramidal cells by in utero DNA electroporation of Long-Evans rat embryos at E18 (Saito and Nakatsuji, 2001; Tabata and Nakajima, 2001; Petreanu et al., 2007; Miyashita et al., 2010). The separate GFP plasmid was needed to drive sufficient fluorescence for transcranial identification of P1 pups with strong S1 expression. We confirmed histologically that fluorescence expression was confined to L2/3 pyramidal cells and their axons, with no expression in L4 or L5 neurons (Figures 1A and 1B). As expected, 100% of fluorescent cells had pyramidal morphology (n = 399 neurons, four histological sections, two rats). Overall, 21.1% ± 0.9% of L2/3 neurons (identified by immunostaining for Neu-N) also expressed fluorescence in the EYFP/GFP emission band (Figure 1C) (n = 10 rats, 37 columns), consistent with a prior study in mouse S1 (Adesnik and Scanziani, 2010). Linear spectral unmixing of GFP and EYFP signals (Zeiss 780 confocal with multispectral detector) confirmed strong EYFP expression in axonal and dendritic membranes (data not shown).

Optogenetic Activation of L2/3 Recurrent Circuits

Circuit function was studied in acute S1 slices prepared at P17–P21. Slices were cut in the "across-row" plane that allows identification of columns corresponding to A–E whisker rows using transillumination (Finnerty et al., 1999). Whole-cell recordings were targeted to presumptive ChR2-expressing or ChR2-nonexpressing cells based on DsRed fluorescence. This approach avoids unwanted ChR2 activation by GFP excitation light. We confirmed in histological sections that 94% ± 1% of DsRed+ L2/3 pyramidal cells also exhibited fluorescence in the EYFP/GFP emission band (n = 1,421 neurons, 37 columns, 10 rats). Moreover, all DsRed+ cells exhibited direct ChR2-mediated photocurrent when patched (see below). Thus, single cells expressed multiple plasmids, and DsRed fluorescence was a valid indicator for putative ChR2+ neurons.

Only slices with strong, uniform expression of DsRed across all S1 columns were used (Figure 2A). A 443 nm blue laser beam (CrystaLaser DL-445-040) was shaped using a pinhole and focusing optics and was routed through a 4× air objective to the slice. Beam diameter (2 SD of Gaussian profile) was either 312 μm (spike threshold experiment) or 238 μm (synaptic physiology experiments), both of which fit in a single column (diameter 375–500 μm; Wimmer et al., 2010).

We first measured ChR2-elicited spike thresholds to determine the light stimulation parameters that achieve single-column photostimulation in L2/3. We made whole-cell current clamp recordings from DsRed+ (putative ChR2+) neurons (n = 13) in L2/3 of the C column and applied 2 ms light pulses centered in L2/3 of either the C column or adjacent columns (Figure 2B). Synaptic transmission was intact, so that both direct photocurrent and network synaptic activation contributed to spiking. At each stimulation site, we identified the threshold photostimulation intensity required to elicit a single spike from V_{rest} (Figure 2C). In the home column, low-intensity light (0.2 ± .05 mW) evoked spikes in every DsRed+ neuron, with < 0.2 ms latency to initial (subthreshold) depolarization. This latency is too short to be mediated

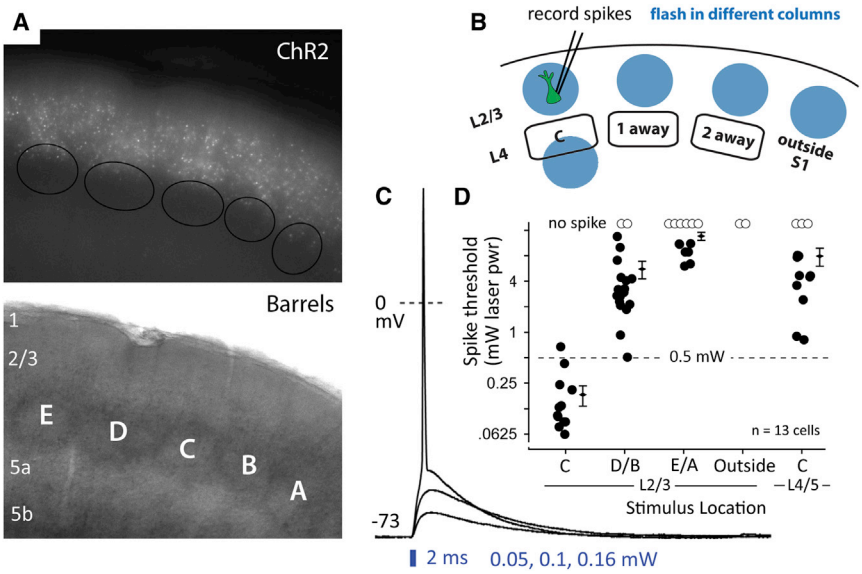

Figure 2. Single-Column Activation of L2/3 Recurrent Networks

(A) Ds-Red epifluorescence in a living slice, with barrels visualized by transillumination.

(B) Schematic of the spike threshold experiment used to calibrate single-column stimulation.

(C) Photostimulation-evoked depolarization and spiking in one DsRed+ pyramidal cell to light stimulation centered in L2/3 of the C column.

(D) Photostimulation intensity required to evoke a spike as a function of photostimulus location. Each circle is a cell. Diamonds and error bars show population mean and SEM.

See also Figure S1.

synaptically and is indicative of ChR2 expression in the recorded neuron (Cruikshank et al., 2010). Higher photostimulation intensity (>0.5 mW) was required to evoke spikes from stimulation sites in adjacent columns and at the L4-L5 border in the home column (Figure 2D). Thus, 2 ms light impulses of <0.5 mW in L2/3 drive spikes in L2/3 pyramidal cells only within a single S1 column. All subsequent experiments used light intensity within the column-specific range.

Synaptic Responses from the L2/3 Recurrent Network

To measure the functional output of the L2/3 recurrent network, we made voltage-clamp recordings from DsRed-negative L2/3 pyramidal neurons and measured excitatory postsynaptic currents (EPSCs) and inhibitory postsynaptic current (IPSCs) evoked by light centered in L2/3 of the neuron's home column. D-APV (50 μM) and saclofen (100 μM) were bath applied to isolate AMPAR-EPSCs and $GABA_A$-IPSCs. EPSCs and IPSCs were measured at −68 and 0 mV, respectively (E_{Cl} and E_{AMPA} in our solutions). Unlike DsRed+ cells, which uniformly exhibited short-latency responses (<0.2 ms), most DsRed− cells exhibited long-latency responses (>1.5 ms) consistent with network-mediated synaptic currents (Figure 3A). Synaptic responses were only analyzed in long-latency cells that lacked direct ChR2 photocurrent. We confirmed that ChR2-evoked EPSCs were blocked by NBQX (10 μM), but not gabazine (1 μM), whereas IPSCs were blocked by both NBQX and gabazine (applied independently), as expected for disynaptic GABA-A inhibition (n = 4 cells) (Figure S1A available online). TTX (1 μM) completely blocked ChR2-evoked currents (n = 4 cells), indicating that synaptic currents were not due to direct ChR2-mediated release from terminals (Figure S1B). Pharmacologically isolated EPSCs and IPSCs reversed at 0.4 ± 2.5 mV and −66.7 ± 0.8 mV (n = 5 and 6 cells) (Figures S1C and S1D), confirming that recording at −68 and 0 mV isolated EPSCs and IPSCs, respectively.

Prior studies of synaptic activation within the local L2/3 recurrent network in S1 focused on output of a single pyramidal cell (Reyes et al., 1998; Feldmeyer et al., 2006; Lefort et al., 2009), recruitment of inhibition by spiking of 1–2 pyramidal cells (Kapfer et al., 2007), or excitation-inhibition balance evoked by strong or sustained network activation (Adesnik and Scanziani, 2010; Mateo et al., 2011). How progressive activation of the L2/3 pyramidal cell population recruits recurrent excitation and inhibition is unknown. We therefore first characterized recruitment of recurrent excitation and inhibition in response to increasing photostimulation of the ChR2-expressing L2/3 pyramidal cell population. Experiments were performed in whisker-intact B columns from P17–P21 rats that had the D row of whiskers plucked for plasticity experiments (see below).

For each neuron (n = 10), we identified the excitatory stimulation threshold (E_{thresh}), defined as the photostimulation intensity that reliably evoked a detectable EPSC. We used a 2 ms light pulse to mimic transient sensory-driven spiking (Simons, 1978; Jadhav et al., 2009). IPSCs were invariably absent at E_{thresh}. Increasing photostimulation intensity (in multiples from 1.0 to 2.0 × E_{thresh}) evoked steadily larger EPSCs (quantified as charge integrated over the first 50 ms of the response) but more steeply larger IPSCs (Figures 3B–3D). IPSC charge increased particularly steeply between 1.0 and 1.4 × E_{thresh}, consistent with supralinear recruitment of a subset of recurrent inhibition (Kapfer et al., 2007). To compare relative recruitment of excitation and inhibition, we calculated fractional excitation (defined as E/(E + I)) at each stimulus intensity. Fractional excitation varied inversely with stimulus intensity, reflecting preferential recruitment of inhibition over excitation as L2/3 network activation increased (Figures 3C–3E).

To determine the relationship between light intensity and spiking in the L2/3 network, we first measured how E_{thresh} for ChR2-negative cells compares with spike threshold for ChR2-positive cells in the same column (n = 7 columns, 21 ChR2- cells, 20 ChR2+ cells). All cocolumnar ChR2− cells had similar E_{thresh}, but intermixed ChR2+ cells showed a range of spike thresholds from 1.0 to 2.0× mean E_{thresh} for the ChR2− cells in that column (Figure S2A). This is expected because each pyramidal cell receives excitatory synapses from many neighbors, so E_{thresh} in ChR2− cells must approximate the lowest spike threshold of local ChR2+ cells. As photostimulus intensity was increased

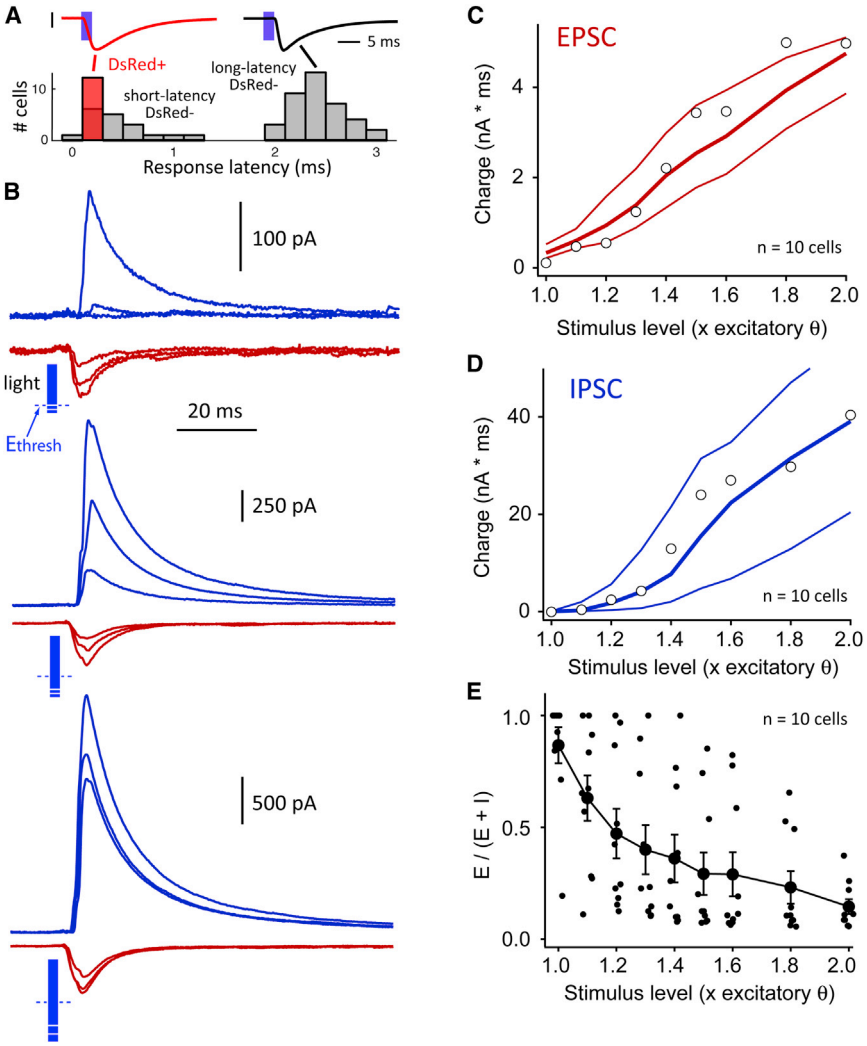

Figure 3. Activation of the Recurrent L2/3 Network by a 2 ms Light Pulse

(A) Bimodal distribution of response latency allowed identification of directly light-responsive versus synaptically responsive cells. Gray bars, DsRed-negative cells under normal recording conditions. Red bar, DsRed+ cells with TTX, kynurenic acid, and PTX present in the bath (in addition to the standard APV and saclofen).

(B) Recruitment of recurrent EPSCs (red) and IPSCs (blue) in an example neuron. Each trace is mean of 10–14 sweeps. Top: 1.0, 1.1, and 1.2 × E_{thresh}. Middle: 1.3, 1.4, and 1.5 × E_{thresh}. Bottom; 1.6, 1.8, and 2.0 × E_{thresh}. Blue bar length indicates photostimulus intensity relative to E_{thresh} (dashed line). Cell was located in B column.

(C and D) EPSC and IPSC charge as a function of light intensity, for all cells in B columns (n = 10 cells). Open symbols show cell in (B). Lines are bootstrapped 25th, 50th, and 75th percentiles.

(E) Fractional excitatory charge for all cells in B columns. Error bars are SEM.

See also Figure S2.

from 1.0 to 2.0× mean column E_{thresh}, the fraction of ChR2+ cells that spiked increased nearly linearly (Figure S2A), but ChR2− cells were not recruited to spike (0/15 cells, six columns). Thus, ChR2 stimulation does not drive positive-feedback recruitment of the L2/3 pyramidal cell network. This was due to powerful disynaptic IPSPs (Figure S2B) that prevented spiking in ChR2− pyramidal cells, as shown previously for ChR2 activation of the L2/3 network in vivo (Mateo et al., 2011). Both fast-spiking (FS) and non-FS L2/3 interneurons are known to mediate this recurrent inhibition (Mateo et al., 2011).

Effects of Whisker Deprivation

To drive whisker map plasticity, the D row of whiskers was plucked from P12 until the day of recording (P17–P21). This manipulation drives weakening of principal whisker-evoked spiking responses in L2/3 of deprived columns, which is a major component of plasticity in juveniles (Glazewski and Fox, 1996; Feldman and Brecht, 2005; Drew and Feldman, 2009). To understand how L2/3 recurrent network function is altered by deprivation, we compared ChR2-evoked synaptic responses in deprived (D) columns with spared (B, C, and E) columns. Example cells from the B and D columns of a single slice are shown in Figure 4. In the B column, EPSCs grew slowly with photostimulation intensity, whereas IPSCs grew more steeply, so that inhibition dominated excitation for all photostimulation intensities >1.2× E_{thresh}. In the D column, EPSCs were recruited similarly, but IPSCs were undetectable until 1.5× E_{thresh}, and inhibition did not exceed excitation until 1.8× E_{thresh}. To rule out differences in functional expression of ChR2 between columns, we recorded the local field potential evoked by photostimulation in the presence of TTX, kynurenic acid, picrotoxin, D-APV, and saclofen to block spikes and fast synaptic transmission. This "photocurrent-local field potential (LFP)" reflects summed photocurrents from the population of pyramidal neurons near the field potential pipette. Photocurrent-LFP magnitude was identical in the two columns across a wide range of photostimulation intensities (Figure 4C).

Across cells, IPSC charge was smaller in D columns than B columns across a wide range of photostimulation intensity ($p < 0.000001$, two-factor ANOVA, B versus D, n = 10 cells each). The largest reductions were observed for $IPSC_{1.1}$ to $IPSC_{1.4}$, with 96.7% smaller IPSCs, on average, in D columns (Figure 5A). EPSC charge was also reduced ($p < 0.001$, two-factor ANOVA, B versus D) but by a smaller amount ($EPSC_{1.1}$ – $EPSC_{1.4}$ were 41.5% smaller in D than in B columns). To take $IPSC_{1.4}$ and $EPSC_{1.4}$ as examples (Figure 5B), $IPSC_{1.4}$ was 92% smaller in D than in B columns (D: 69 ± 29 pA peak, 1.4 ± 0.4 nA*ms charge; B: 880 ± 352 pA peak, 13.9 ± 5.4 nA*ms charge, $p < 0.05$, t test). $EPSC_{1.4}$ was 45% smaller in D than in B columns (D: 139 ± 37 pA peak, 1.2 ± 0.27 nA*ms charge; B: 272 ± 53 pA peak, 2.2 ± 0.4

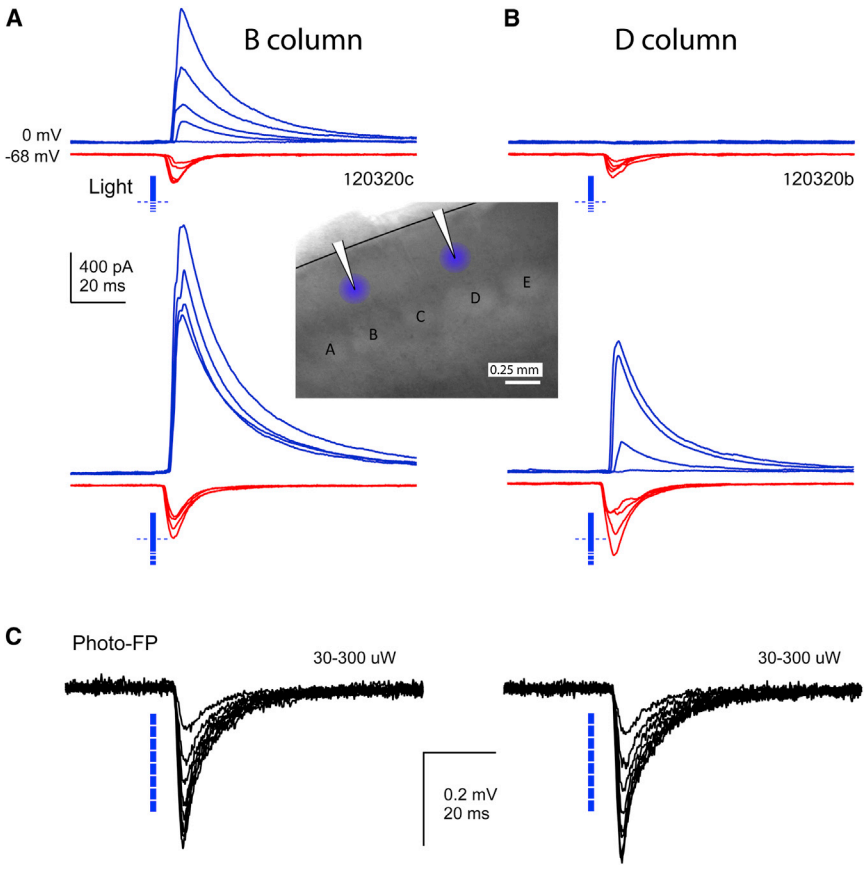

Figure 4. Effect of D-Row Deprivation on Two Representative Cells in B and D Columns of a Single Slice

(A and B) IPSCs (blue) and EPSCs (red) recorded in response to 1.0 – 1.4 × E_{thresh} (top) and 1.5, 1.6, 1.8, and 2.0 × E_{thresh} (bottom). Inset: recording and photostimulus locations for these two neurons.

(C) Photocurrent-LFPs recorded at the location of each neuron in the presence of TTX, kynurenic acid, and picrotoxin. Photocurrent-LFPs were recorded in response to the same series of photostimulation intensities (30–300 μW) and were identical in both columns.

nA*ms charge, $p < 0.05$ and $p = 0.054$, respectively). In contrast, there was no difference in V_{rest} (B: −69.5 ± 1 mV D: −68.3 ± 2 mV, $p = 0.6$, t test) or R_{input} (at −68 mV, B: 329 ± 50 MΩ; D: 279 ± 31 MΩ, $p = 0.4$) (Figure 5B, inset). To determine whether excitation-inhibition ratio was changed, we calculated fractional excitation (E/(E + I)) for each cell and stimulation intensity. Fractional excitation was significantly higher in D than in B columns at 1.1–1.4× E_{thresh} (two-factor ANOVA, deprivation effect $p = 0.001$, interaction $p < 0.05$, Tukey HSD post hoc test, $p < 0.05$ for 1.1–1.4× E_{thresh}) (Figure 5C).

These changes in network-mediated synaptic responses occurred without systematic differences in direct ChR2 photocurrent (as assayed by photocurrent-LFP amplitude at E_{thresh}) or in the ability of light stimulation to drive initial EPSCs (assayed by the laser intensity required to elicit $EPSC_{1.0}$), indicating that ChR2 activation was equally effective in driving spikes in ChR2+ cells in D versus in B columns (Figure 5D). To determine whether deprivation effects were confined to deprived D columns, we recorded neurons (n = 10) in spared C and E columns, using a subset of stimulus intensities (1.0, 1.2, and 1.3× E_{thresh}). EPSCs and IPSCs in C and E columns were identical to B columns (ANOVA, $p > 0.05$) and were larger than in deprived D columns (ANOVA, $p < 0.05$) (Figure 5B, inset). Again, ChR2 activation was equally effective in C/E versus D columns (Figure 5D). Together, these results indicate that D-row deprivation powerfully reduced recurrent inhibition in L2/3 of deprived columns and more modestly reduced recurrent excitation.

Effect of Deprivation on Network Oscillations In Vitro

A major function of local recurrent inhibition, particularly via fast-spiking (FS) interneurons, is to synchronize spiking activity in the gamma frequency band, generating oscillations that are measurable both intracellularly and in local field potentials (Cardin et al., 2009; Buzsáki and Wang, 2012). Gamma oscillations have been proposed to promote synaptic integration, to select or bind cell assemblies, and to enable efficient area-to-area coupling for information transfer (Fries, 2009; Wang, 2010). Gamma occurs in awake rodent S1 (Sirota et al., 2008; Pritchett et al., 2012, Soc. Neurosci., abstract, 377.11), but its functional role there is not understood. We predicted that reduced recurrent inhibition may reduce the capacity of L2/3 to generate gamma oscillations.

To measure gamma oscillations within L2/3 recurrent circuits, we photostimulated with light ramps (1.2 s duration, linear ramp to 2.5, 5, or 10× E_{thresh}, 238 μm spot diameter centered in L2/3 of one column). Calibration experiments showed that these ramps evoked spikes largely in the home column (Figure S3). We made voltage-clamp recordings from DsRed-negative pyramidal cells and measured ramp-evoked EPSCs and IPSCs. In spared B columns (n = 16 cells), evoked IPSCs (measured at 0 mV) showed prominent oscillations in the low gamma range (20–60 Hz), as shown previously in slices from whisker-intact mice (Adesnik and Scanziani, 2010). Evoked EPSCs (measured at −68 mV) had substantially less gamma power (Figure 6A). In deprived D columns (n = 16 cells), the sustained component of the IPSC was attenuated and gamma oscillations were substantially reduced (Figures 6B–BF). This was true for all ramp intensities. For $IPSC_{10}$, the sustained component (0.3–1.2 s after ramp onset) was 68% smaller in D columns (B: 142 ± 27 pA; D: 45 ± 17 pA) and had 70% less gamma power (mean in 20–60 Hz band; B: 43.4 ± 14 pA^2; D: 12.9 ± 6.4 pA^2 in D columns), whereas the early peak (0–0.3 s) was not much affected (B: 611 ± 73 pA; D: 497 ± 80 pA). Two-factor ANOVA (whisker experience × ramp intensity) showed a significant effect of experience on sustained IPSC amplitude ($p < 0.00005$) and gamma power ($p < 0.005$). In contrast, EPSC sustained amplitude was indistinguishable

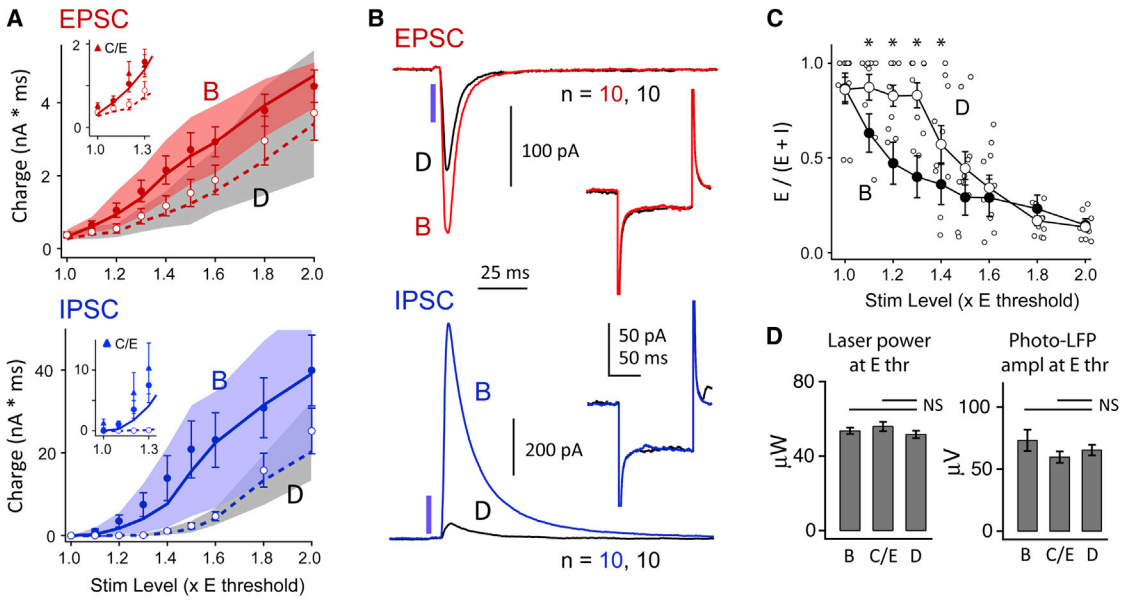

Figure 5. Effect of D-Row Deprivation on Synaptic Responses Elicited by 2 ms Light Pulse

(A) Recruitment of recurrent EPSCs and IPSCs in spared B versus deprived D columns. Circles: mean ± SEM. Lines and shaded region: median and 25th–75th quartiles. Insets: EPSCs and IPSCs measured in spared C and E columns (triangles), relative to B and D columns (circles and lines).

(B) Mean population EPSC and IPSC at 1.4 × E_{thresh} in B and D columns (n = 10 cells each). Inset: the average response to a −5 mV current step was not altered by deprivation.

(C) Fractional excitatory charge was higher in D columns, consistent with reduced IPSCs. *p < 0.05, Tukey HSD. B column mean (not individual cells) is replotted from Figure 3E.

(D) Mean effective stimulation intensity was not different between B and D columns, as assessed by laser intensity required to elicit a threshold EPSC or by amplitude of photocurrent-LFP at E_{thresh}.

Error bars are SEM.

between spared and deprived columns (ANOVA, p > 0.05), and EPSC gamma power showed a modest decrease (Figures 6C and 6E) (p < 0.05). Thus, deprivation powerfully reduced the ability of L2/3 local circuits to generate endogenous gamma oscillations.

Spontaneous Network Oscillations In Vivo

To test whether reduced oscillations also occurred in vivo, we measured spontaneous LFPs in spared and deprived S1 cortical columns in urethane anesthetized rats. Rats (n = 5) were deprived of D-row whiskers from P12, and recordings were made at P30–P37 after 14 days deprivation followed by 4–11 days of partial whisker regrowth. LFP recordings (500 ms duration) were made in L4 and L2/3 of D (deprived) and C or E (spared) columns in each animal (Figures 7A and 7B). Spontaneous LFPs were dominated by low frequencies but included periods with enhanced gamma power (Figure 7B, bold epochs), as observed previously (Cardin et al., 2009). We compared LFP spectra between spared and deprived columns within each animal by normalizing all spectra to the average peak gamma power (30–50 Hz band) measured in spared columns for that animal. For L2/3, the resulting normalized spectra (averaged across animals) show that spectral power was reduced in deprived columns across a broad range of frequencies, with maximal decrease of 26% ± 12% in the 30–40 Hz range (n = 3,070 sweeps in 14 deprived columns, 2,617 sweeps in 11 spared columns, 5 rats). Power was significantly decreased in all gamma frequencies (20–80 Hz, tested in 10 Hz bands, α = 0.05, permutation test) (Figure 7D). This effect was consistent in 4/5 animals (Figure 7E). Reduced gamma power was observable in raw LFPs as reduced LFP amplitude during gamma-containing epochs (Figure 7B). In contrast, in L4 of the same penetrations, deprivation had no effect on average gamma power (3162 sweeps in deprived columns, 2,517 sweeps in spared columns, Figures 7C and 7D). Thus, deprivation decreases spontaneous (resting) gamma in L2/3 in vivo. We did not analyze whisker deflection-evoked gamma because any reduction is trivially attributed to the weakened L4 input to L2/3 (Allen et al., 2003; House et al., 2011).

DISCUSSION

L2/3 is a major locus of whisker map plasticity in postneonatal rodents (Fox, 2002; Feldman, 2009), but prior studies of cellular plasticity mechanisms in L2/3 have focused on excitatory circuits almost exclusively. Whisker deprivation alters cross-columnar excitation (Finnerty et al., 1999; Marik et al., 2010), L4-L2/3 feedforward excitation (Allen et al., 2003; Shepherd et al., 2003; Clem and Barth, 2006; Bender et al., 2006; Hardingham et al., 2008; House et al., 2011), and local recurrent excitation in single columns (Cheetham et al., 2007, 2008; Bruno et al., 2009; Wen and Barth, 2011). These excitatory circuit

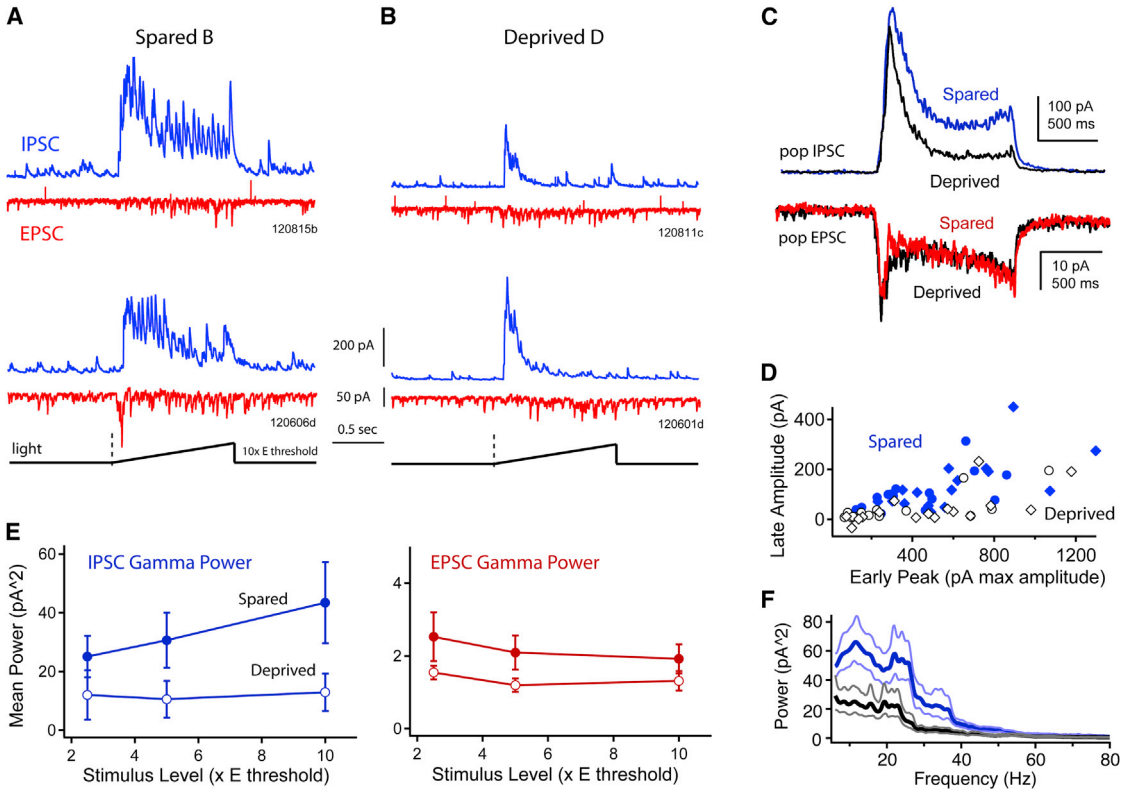

Figure 6. Effect of Deprivation on Intrinsic Gamma Oscillations Evoked by Ramp Photostimulation

(A) Two example B column cells, showing EPSCs and IPSCs evoked by a light ramp to 10 × E_{thresh}. Each trace is a single sweep.

(B) Two example D column cells, using the identical light ramp.

(C) Population mean EPSC and IPSC in spared (B) versus deprived (D) columns, calculated for 10 × E_{thresh} stimuli.

(D) Effect of deprivation on early IPSC amplitude versus late IPSC amplitude (0–0.3 and 0.3–1.2 s after ramp onset). Each symbol is one cell tested at 5 × E_{thresh} (circles) or 10 × E_{thresh} (diamonds).

(E) Mean gamma power (20–60 Hz) for late component of IPSCs and EPSCs. Bars are SEM.

(F) Mean power spectrum for late IPSCs in spared B columns (blue) versus deprived D columns (black), for 10× E_{thresh} ramps.

See also Figure S3.

changes are mostly consistent with reduced feedforward and local excitation within deprived columns, increased feedforward excitation into spared columns, and increased cross-columnar excitation from spared to deprived columns. These are appropriate to explain basic Hebbian features of map reorganization, including the reduction in responses to deprived whiskers and the strengthening and expansion of spared whisker representations.

In contrast, the role of L2/3 inhibitory circuits in plasticity is not understood. We hypothesized that deprivation preferentially weakens local recurrent inhibition in L2/3 relative to excitation. This disinhibition would constitute a homeostatic (compensatory) response to whisker deprivation (Turrigiano, 2012), which would be a significant modification of classical Hebbian models of L2/3 plasticity (e.g., Buonomano and Merzenich, 1998). Recently, in vivo measurements have detected deprivation-induced disinhibition in whisker-evoked sensory responses in L2/3 of S1 (Li and Feldman, 2010, Soc. Neurosci., abstract, 284.1; Gambino and Holtmaat, 2012). However, whether L2/3 recurrent circuits are a site of this disinhibition was not known.

We used ChR2 activation of L2/3 pyramidal cells to measure AMPA-mediated excitation and GABA-A mediated inhibition in local L2/3 recurrent networks (Adesnik and Scanziani, 2010; Mateo et al., 2011). Whisker deprivation moderately reduced L2/3 recurrent excitation (by ~40%, for $EPSC_{1.1–1.4}$), consistent with the known reduction in PYR-PYR local connectivity (Cheetham et al., 2007). However, a much larger decrease (~95%) was observed for recurrent inhibition, resulting in a substantial increase in excitation-inhibition ratio. These effects were observed in deprived D columns relative to spared B, C, and E columns, suggesting that disinhibition was column specific. Increased excitation-inhibition ratio was most pronounced at stimulus levels of 1.1–1.4× E_{thresh}, corresponding to initial network recruitment (Figure 5). This is likely to be the most physiologically relevant activity regime, because L2/3 neurons spike sparsely in vivo (Jadhav et al., 2009; O'Connor et al., 2010). Thus, L2/3 recurrent circuits are a major site of disinhibition following whisker deprivation and of homeostatic plasticity within deprived columns. We do not know how NMDA- or GABAB-receptor mediated currents were affected by deprivation.

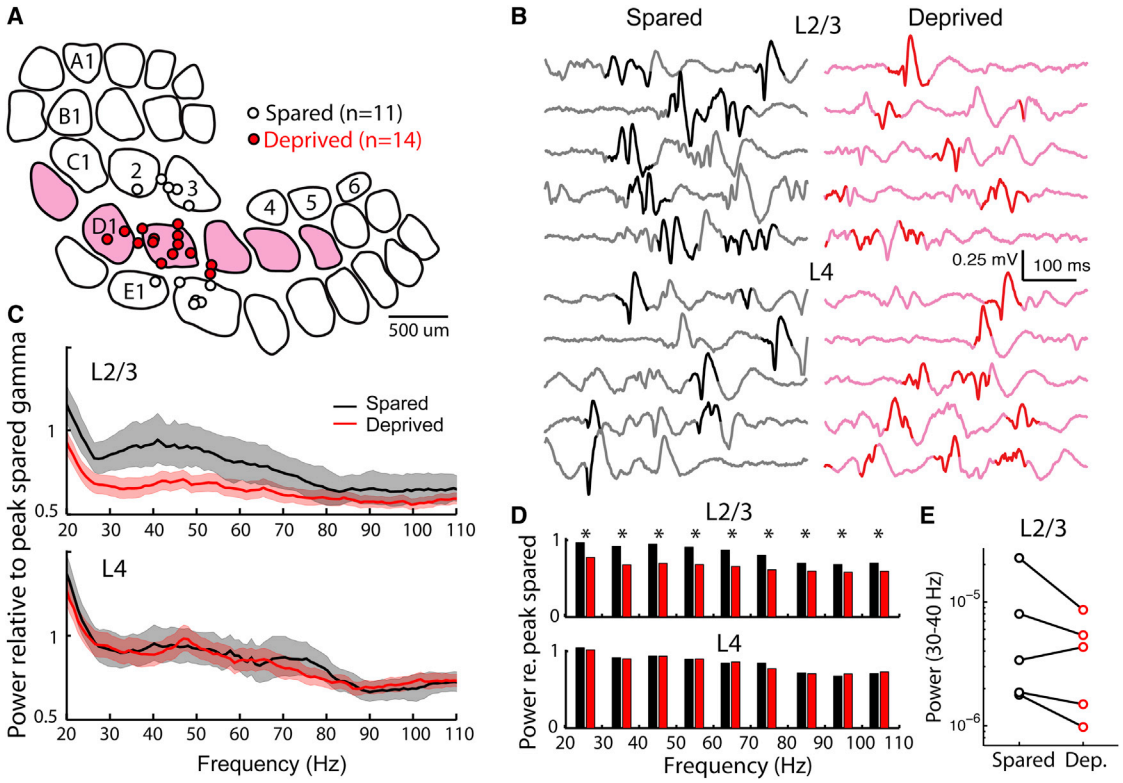

Figure 7. D-Row Deprivation Reduces Spontaneous Gamma Oscillations in L2/3 of Anesthetized S1 In Vivo.

(A) Recording locations for deprived (D) and spared (C and E) penetrations, reconstructed from marking lesions and plotted on representative barrel outlines. Deprived columns are shaded.

(B) Example raw LFP traces from a spared and a deprived column of one animal. Traces were chosen based on maximum similarity to mean LFP spectra for this animal. Bold indicates LFP segments with highest 40 Hz power (see the Experimental Procedures).

(C) Mean normalized LFP spectra for spared and deprived columns across all animals. Shading: 99% confidence intervals.

(D) Mean normalized LFP power in 10 Hz bins. Top: L2/3 recordings. Bottom: L4 recordings. *$p < 0.05$, random permutation test.

(E) Mean LFP power in 30–40 Hz band for L2/3 recordings in each of the five rats separately.

Optogenetic stimulation provided several key advantages to examine changes in recurrent circuit function after experience-dependent plasticity. Optogenetic activation was critical to enable selective, single-column activation of the L2/3 recurrent network without contamination from fibers of passage, feedforward input, or direct stimulation of interneurons. Furthermore, graded stimulation by increasing light intensity allowed us to characterize the progressive recruitment of excitation and inhibition in the active recurrent network, which provides substantial additional information beyond unitary synaptic physiology using dual whole-cell recording. Light ramp stimulation confirmed that recurrent inhibition was reduced substantially more than excitation and showed that the ability of deprived L2/3 networks to generate gamma oscillations was profoundly reduced (Figure 6). This reduction was also observed in vivo, suggesting that L2/3 network changes are physiologically relevant (Figure 7). In contrast, prior studies of recurrent circuit plasticity were restricted to selected unitary connections or inferred recurrent network function from spontaneous activity, which is relatively nonselective and influenced by multiple circuit components (Cheetham et al., 2007; Maffei et al., 2004, 2006).

Reduced Inhibition as a Homeostatic Mechanism during Critical Period Plasticity

Deprivation is known to weaken or delay early development of inhibition in L4 (Chattopadhyaya et al., 2004; Maffei et al., 2004; Jiao et al., 2006; Chittajallu and Isaac, 2010), but its effects during the critical period for plasticity and in L2/3 have been unclear. Visual deprivation during the critical period potentiates recurrent inhibition in L4 of V1 (Maffei et al., 2006), but evidence for such potentiation in L2/3 or in S1 has been lacking. We performed deprivation during the P10–P14 critical period for maximal L2/3 plasticity in S1 (Stern et al., 2001) and found that L2/3 recurrent inhibition was strongly reduced. This is consistent with several structural measures of plasticity in L2/3 interneurons (Marik et al., 2010; Chen et al., 2011; Keck et al., 2011; van Versendaal et al., 2012) and provides a circuit locus for the disinhibition observed in vivo for whisker-evoked sensory responses in L2/3 of deprived (Li and Feldman, 2010, Soc. Neurosci., abstract, 284.1) and spared (Gambino and Holtmaat, 2012) columns. Thus, the current results show that L2/3 recurrent circuits are a major site of disinhibition for critical period plasticity. The preferential reduction in inhibition is unlike the L4-L2/3 feedforward

projection, where deprivation drives a parallel (balanced) reduction in excitation and inhibition (House et al., 2011). Because local recurrent inhibition was not reduced in spared columns (Figure 5), disinhibition to surround whiskers in spared columns in vivo (Gambino and Holtmaat, 2012) must reflect either reduced cross-columnar drive onto local L2/3 interneurons or reduced efficacy of cross-columnar inhibitory axons (Helmstaedter et al., 2009). Deprivation also weakens L4-L2/3 feedforward inhibition in V1 and increases L2/3 network excitability, but whether local recurrent circuits are affected is not known (Maffei and Turrigiano, 2008).

Preferential reduction of L2/3 inhibition will increase network excitability and promote whisker-evoked spiking and therefore is a homeostatic response to deprivation that co-occurs with Hebbian weakening of excitatory input (Turrigiano, 2012). Reduced inhibition may also broaden sensory tuning, depending on which interneuron subtypes are affected (Atallah et al., 2012; Wilson et al., 2012). Deprivation-induced disinhibition in L2/3 of S1 also promotes LTP of spared whisker responses (Gambino and Holtmaat, 2012) and thus may be a permissive gate for subsequent steps in whisker map plasticity (Gandhi et al., 2008; Yazaki-Sugiyama et al., 2009; House et al., 2011). Consistent with this idea, disinhibition precedes associative learning and receptive field plasticity in L2/3 of auditory cortex (Froemke et al., 2007; Letzkus et al., 2011), and reduction of inhibition restores ocular dominance plasticity in adult V1 (Sale et al., 2010).

Sites and Mechanisms for Inhibitory Plasticity

Reduced recurrent excitation and inhibition may represent the functional outcome of known structural plasticity in L2/3 circuits. Deprivation reduces PYR-PYR unitary connection rate in deprived columns by reorganization of synaptic contacts and local axons (Cheetham et al., 2007, 2008; Bruno et al., 2009) without altering intrinsic excitability or unitary EPSP amplitude (Allen et al., 2003; Bender et al., 2006; Cheetham et al., 2007). This is likely to underlie the reduction in L2/3 recurrent excitation. In addition, deprivation drives rapid loss of inhibitory cell axons (in S1; Marik et al., 2010), dendritic and spine retraction by L2/3 interneurons, loss of inhibitory axonal boutons, and loss of inhibitory synapses on PYR dendrites (in V1; Chen et al., 2011; Keck et al., 2011; van Versendaal et al., 2012). These changes are likely to contribute to the loss of L2/3 recurrent inhibition observed here. Reduced inhibition may also reflect physiological weakening of excitatory synapses onto L2/3 interneurons (Lu et al., 2007).

Many inhibitory cell types exist in L2/3 that could mediate the loss of recurrent inhibition (Gentet, 2012). One likely candidate is FS basket cells, which contribute strongly to disynaptic inhibition elicited by brief ChR2 stimulation in L2/3 pyramidal cells (Mateo et al., 2011) and generate perisomatic recurrent inhibition. Deprivation increases FS→PYR unitary IPSPs and does not alter FS intrinsic excitability (House et al., 2011), suggesting that reduced recurrent inhibition to the 2 ms pulse may reflect a reduction in the strength or number of PYR→FS synapses. This is also consistent with the loss of gamma oscillations (see below). We speculate that recurrent inhibition evoked by ramp stimuli also involves somatostatin-positive Martinotti cells, which generate dendritic inhibition (Reyes et al., 1998; Kapfer et al., 2007). The reduction in ramp-evoked inhibition may reflect reduced activation or output of these cells, including structural loss of dendritic inhibitory synapses.

Plasticity of Gamma Oscillations

A major function of L2/3 FS inhibitory networks is to synchronize PYR cell spiking in the gamma frequency range (Cardin et al., 2009; Sohal et al., 2009). Gamma oscillations are a characteristic feature of cortical processing and have been proposed to promote synaptic integration, bind activity in cell assemblies, and regulate information transfer between neighboring neurons and distant cortical areas (Fries, 2009; Sohal et al., 2009; Wang, 2010). In rat S1, short bursts of tightly spatially localized gamma occur during exploration, though their behavioral relevance remains unclear (Sirota et al., 2008). Synaptic plasticity within PYR-FS circuits has been proposed to alter gamma oscillations (Paik and Glaser, 2010), but experimental evidence for plasticity of gamma (or other cortical rhythms) is lacking. We hypothesized that by reducing L2/3 inhibition, deprivation may reduce the capacity for gamma oscillations in deprived columns. Indeed, we observed a 70% reduction in ramp-evoked gamma power in L2/3 of S1 slices and a 25% reduction in spontaneous gamma power in L2/3 of deprived columns in S1 in vivo (Figures 6 and 7). Thus, the capacity for gamma oscillations is plastic and depends on sensory experience, likely reflecting local plasticity in FS recurrent circuits.

We speculate that this reduction in gamma power may impair sensory computation and reduce the ability of deprived whisker input to be relayed to higher cortical areas. If so, this would act to reduce the effective perceptual impact of deprived whiskers beyond the Hebbian reduction in whisker-evoked spike count alone. Thus, modulation of gamma could be an additional mechanism by which sensory experience regulates sensory processing or perception.

Conclusion

We used optogenetics to investigate the functional recruitment of L2/3 recurrent circuits during deprivation-induced whisker map plasticity. Deprivation modestly reduced recurrent excitation but powerfully reduced recurrent inhibition, suggesting that L2/3 recurrent circuits are a major site of homeostatic plasticity. At the same time, the capacity for gamma oscillations were powerfully reduced, which is likely to reduce the effective representation of deprived whiskers.

EXPERIMENTAL PROCEDURES

Long-Evans rats (both sexes) were used. Procedures were approved by UC Berkeley Institutional Animal Care and Use Committee and meet the National Institutes of Health's guidelines.

In Utero Electroporation

Timed-pregnant rats (18 days postcoitum) were anesthetized with isoflurane. The uterus was lifted from the abdominal cavity, and embryos were visualized and electroporated through the uterine wall. A glass pipette (30–40 μm tip diameter) was placed inside the left lateral cerebral ventricle, and ~1 μl of plasmid DNA solution was injected. The DNA solution contained: pCAG-ChR2(H134R)EYFP-WPRE plasmid (1 μg/μl), pCAG-DsRed plasmid (0.5 μg/μl), pCAG-GFP (0.5 μg/μl) plasmid, and 0.05% Fast Green. The capillary was removed, and electrode forceps (CUY650-5; NEPA GENE) were

placed on either side of the head, outside the uterine wall. Five 50 V square pulses (50 ms duration, 950 ms interval) were delivered via an electroporator (BTX ECM830, Harvard Apparatus). The uterus was returned to the abdominal cavity, and the abdominal wall and skin were sutured. Buprenorphine was given for postoperative analgesia (0.05 mg/kg, twice at 8 hr interval). Pups were born by natural delivery.

The purpose of the GFP plasmid was to increase overall fluorescence intensity to enable identification of expressing pups by transcranial imaging at postnatal day (P) 1. Only pups showing strong fluorescence in the EYFP/GFP emission band in S1 on P1 were used in later experiments. The purpose of the DsRed plasmid was to enable fluorescently targeted patching of expressing cells during brain slice physiology (EYFP/GFP fluorescence was not imaged during physiology experiments, to avoid activating ChR2 with GFP excitation wavelengths). All DsRed cells expressed ChR2 (see the Results), indicating that individual cells take up multiple plasmids.

Whisker Deprivation

Starting at postnatal day (P) 12, D-row whiskers D1–D6 and γ were plucked from the right side of the face under transient isoflurane anesthesia (3.5% in O_2). This is a standard manipulation to drive whisker map plasticity in L2/3 of S1 (Drew and Feldman, 2009). Plucking continued every other day (for 5–9 days) until recording.

Slice Preparation

Acute S1 slices were prepared at P17–P21 using standard techniques. Pups were anesthetized with isoflurane; the brain was isolated; and slices (0.4 mm) were cut in a semicoronal plane (Feldmeyer et al., 2002) that allows identification of A–E whisker columns (Finnerty et al., 1999; Allen et al., 2003). Slices were cut in low-sodium cutting solution (mM: NaCl 85, sucrose 75, D-(+)-glucose 25, $NaHCO_3$ 25, KCL 2.5, NaH_2PO_4 1.25, ascorbic acid 0.5, $MgCl_2$ 4, $CaCl_2$ 0.5, bubbled with 95:5 O_2:CO_2 [pH 7.2]) and collected into standard Ringer's solution (mM: 119 NaCl, 26.2 $NaHCO_3$, 11 D-(+)-glucose, 1.3 $MgSO_4$, 2.5 KCl, 1 NaH_2PO_4, and 2.5 $CaCl_2$). Slices were incubated 30 min at 32°C and then stored 1–4 hr at room temperature (RT) before use. Column boundaries were identified with transillumination.

In each slice, the spatial extent and level of expression were evaluated by visualizing DsRed fluorescence with low-power epifluorescence imaging using a Rolera XR camera (Q Imaging). (DsRed was used to avoid GFP excitation, which activates ChR2.) Only slices with strong, spatially uniform DsRed expression over all five barrels of S1 (e.g., Figure 2A) were used in experiments. Whole-cell recordings were targeted to presumptive ChR2-expressing or ChR2-nonexpressing cells based on DsRed fluorescence using a 40× objective. In histological sections (n = 37 columns, ten rats), we determined that 94% ± 1% of DsRed+ L2/3 pyramidal cells also showed EYFP/GFP fluorescence, and 100% of DsRed+ cells showed direct ChR2 photocurrents, indicating that cells took up multiple plasmids (see below). This validates use of DsRed fluorescence to identify putative ChR2+ neurons.

Electrophysiology

Whole-cell recordings were made at 31°C using 2.5–4 MΩ pipettes and a Multiclamp 700B amplifier (Molecular Devices). Current clamp recordings to measure ChR2-evoked spiking were made using K gluconate internal (mM: 116 K gluconate, 20 HEPES, 6 KCl, 2 NaCl, 0.5 EGTA, 4 MgATP, 0.3 NaGTP, 5 Na_2phosphocreatine; pH 7.2 and 295 mOsm). Recordings were made in Ringer's solution. Voltage clamp recordings to measure ChR2-evoked synaptic currents were made using Cs gluconate internal with QX-314 and BAPTA (mM: 108 D-gluconic acid, 108 CsOH, 20 HEPES, 5 tetraethylammonium-Cl, 2.8 NaCl, 0.4 EGTA, 4 MgATP, 0.3 NaGTP, 5 BAPTA, 5 QX-314 bromide; pH 7.2 and 290 mOsm). Pipette capacitance was neutralized, and whole-cell capacitance and series resistance were compensated (prediction and correction, 80%). The bath solution was Ringer's with D-APV (50 μM) and saclofen (100 μM). To measure the photo-LFP associated with direct ChR2 photocurrents, a 1.8–2.2 MΩ field potential pipette was used, and TTX citrate (50 μM), kynurenic acid (2 mM) and picrotoxin (100 μM) were added to the bath. All drugs were from Tocris.

R_{input} and R_{series} were monitored in each sweep in response to a 5 mV test pulse. Recordings were targeted to pyramidal-shaped somata. Cells were excluded if V_m at break-in was >−60 mV, R_{series} >20 MΩ or R_{input} <100 MΩ. V_m values for voltage clamp recordings were corrected for the measured liquid junction potential (12 mV). Data acquisition and analysis used custom software in IGOR Pro (Wavemetrics) and Matlab.

ChR2 Activation

A 443 nm blue laser (40 mW, CrystaLaser DL445-040) was coupled via a multimodal fiber to the microscope epifluorescence arm and projected to the slice through a 4× air objective. Focusing optics and a pinhole set the beam diameter at the slice to 238 μm (2 × SD of Gaussian profile) for synaptic physiology experiments or 312 μm for the spike threshold experiment. Both of these are smaller than the width of a single barrel column in rats (diameter 375–500 μm; Wimmer et al., 2010). Laser intensity and timing were controlled by analog voltage commands generated in IGOR Pro. All laser intensity values represent intensity at the sample, calibrated using a light meter (Newport 1918-C). The lowest possible light intensities were always used to avoid phototoxicity.

Synaptic Responses

Synaptic responses were defined as light-evoked currents with latency >1 ms in nonfluorescent L2/3 pyramidal neurons (see below). Synaptic responses were measured in D-APV (50 μM) and saclofen (100 μM) and thus primarily reflect AMPA and GABA-A currents. The light stimulus was centered in L2/3 of the home column for the recorded neuron. For each cell, we first determined the light intensity (using a 2 ms light pulse) required to elicit a reliable synaptic response, which was invariably an EPSC. This light intensity was defined as excitatory threshold (E_{thresh}).

For cells in the impulse experiment, we measured light-evoked currents at −68 mV (presumed EPSCs) and 0 mV (presumed IPSCs) at 1.0, 1.1, 1.2, 1.3, 1.4, 1.5, 1.6, 1.8, and 2.0 × E_{thresh} to define an input-output curve for synaptic currents (10–14 sweeps at each holding potential and stimulus intensity, 10 s interspike interval [isi]). Note that because driving force is equal for EPSCs and IPSCs, reporting current or conductance is equivalent. PSC magnitude was measured as charge (integrated current) in the first 50 ms of the response, relative to a 2 ms baseline prior to the light stimulus. Fractional excitation (E/(E + I)) was calculated from PSC charge. R_{series} compensation was checked and corrected several times during each recording, and cells were discarded if uncompensated R_{series} exceeded 20 MΩ. For cells in the ramp experiment, we measured currents at −68 and 0 mV in response to a linear ramp of light intensity (1.2 s duration) from 0 mW to 2.5, 5, or 10 × E_{thresh} (five sweeps at each holding potential at each stimulus intensity, 30 s isi). Oscillations were analyzed during the last 900 ms of the ramp stimulus, by calculating power spectra on individual sweeps, in both Igor and Matlab (Chronux toolbox). Gamma in slices was defined as power at 20–80 Hz, which is slightly lower than in vivo (Adesnik and Scanziani, 2010).

In Vivo LFP Recording

D-row whiskers were plucked from P12–P26 under transient isoflurane anesthesia. At P30–P37, rats were anesthetized with urethane (1.5 g/kg i.p., plus 10% maintenance doses as needed). A craniotomy was made over S1 (2.5 mm caudal, 5.2 mm lateral from bregma). LFPs were recorded using a tungsten electrode (5 ± 1 MΩ, FHC), amplified 1,000×, bandpass filtered (10–300 Hz), digitized at 44.1 kHz using custom routines in Igor Pro, and downsampled to 1 kHz offline. Data are from 500 ms spontaneous activity periods (no whisker stimulation) collected every 10 s. A small whisker deflection was applied after each spontaneous period but was not analyzed here. Recording depth was 491 ± 12 μm (n = 24) for L2/3 and 772.8 ± 7 μm for L4 (n = 24), as previously calibrated for Long-Evans rats at this age (Celikel et al., 2004). Penetrations were targeted to both deprived (D) and spared (C or E) columns in each animal, with randomized recording order. Approximately 240 sweeps were recorded in each layer per penetration (L2/3: 237 ± 4 sweeps, L4: 237 ± 9 sweeps). After all recordings were finished, electrolytic lesions were made in L4 (5 μA, 10 s, tip negative), and recording sites were reconstructed relative to barrel boundaries, as revealed by cytochrome oxidase staining in flattened tangential sections (Li et al., 2009). At least one deprived and one spared column was recorded in each animal, enabling within-animal comparison of deprived versus spared column LFPs.

The in vivo gamma experiments used longer deprivation (14 days) than the slice experiments (5–9 days). Deprivation from 7–20 days duration drives similar weakening of whisker responses in L2/3 in vivo (Glazewski and Fox, 1996). While network function and plasticity mechanisms can differ with age, gamma was reduced in both experiments, suggesting it is a conserved feature of plasticity across this age range.

In Vivo LFP Analysis

L2/3 and L4 spectra were analyzed separately. In 2/5 animals, slight 60 Hz recording noise was present, so LFP waveforms were notch filtered at 60 Hz (0.05 dB stopband attenuation, applied to all spared and all deprived recordings in those animals). LFPs were whitened using a second-order autoregression algorithm (Schneider and Neumaier, 2001; Minlebaev et al., 2011) whose coefficients were determined by fitting all LFPs as a group. Spectra were calculated from each whitened LFP segment using the Chronux toolbox in MATLAB (three tapers, 4 Hz bandwidth, 500 ms windows). To compare spectra between deprived and spared columns, all spectra from a single animal were divided by the peak power in the 30–50 Hz band of the average spared spectrum for that animal. These normalized spectra were then averaged across animals to determine the mean normalized spectra in spared and deprived columns. Confidence intervals (99%) were determined by jackknifing (Chronux). Statistical differences were tested for average power in 10 Hz bins using a random permutation test in which spared/deprived labels were randomized without replacement (5×10^5 permutations, $\alpha = 0.05$, Bonferroni correction for multiple comparisons). Representative LFP segments (Figure 7B) were selected as those segments whose spectra showed the minimum least-squared error relative to the average spectrum. The highlighted 40 Hz epochs were identified by band-pass filtering the raw LFP (40 ± 7.5 Hz, Butterworth) and highlighting segments with band-passed amplitude >1 SD above the mean for that layer and condition (spared or deprived).

Histology

Rats were deeply anesthetized with isoflurane and perfused transcardially with 4% paraformaldehyde in 0.1 M phosphate buffer (PB), and the brain was removed. Brains were postfixed for 2 hr, cryoprotected in 30% sucrose in 0.1 M PB, and sectioned (50 μm) coronally on a freezing microtome. To determine the fraction of electroporated cells, sections were costained for the pan-neuronal marker Neu-N by incubating free-floating sections for 40–48 hr at 4°C with mouse anti-NeuN antibody (1:400, Millipore, MAB377) in phosphate-buffered saline (PBS) containing 0.5% Triton X-100 and 5% normal goat serum. Sections were rinsed with PBS and incubated for 90 min at room temperature in Alexa-594 conjugated goat anti-mouse secondary (1:200, Invitrogen). Sections were rinsed three times in PB and mounted in Vectashield. Images were obtained by confocal microscopy (Zeiss LSM 710 Axio Observer).

Statistics

Reported values are mean ± SEM, unless otherwise noted. Medians and 95% confidence intervals were generated by bootstrapping (1,000 resamplings) from the original distributions.

SUPPLEMENTAL INFORMATION

Supplemental Information includes three figures and can be found with this article online at http://dx.doi.org/10.1016/j.neuron.2013.07.026.

ACKNOWLEDGMENTS

We thank Prof. K. Deisseroth (Stanford University) for the ChR2-H134R-EYFP-WPRE construct. This work was supported by grants from the National Institutes of Health (1R01 NS073912) and the National Science Foundation (NSF) (# SMA 1041755) to the Temporal Dynamics of Learning Center, an NSF Science of Learning Center. B.R.I. was supported by National Science Foundation predoctoral fellowship (DGE 1106400).

Accepted: July 10, 2013
Published: October 2, 2013

REFERENCES

Adesnik, H., and Scanziani, M. (2010). Lateral competition for cortical space by layer-specific horizontal circuits. Nature *464*, 1155–1160.

Allen, C.B., Celikel, T., and Feldman, D.E. (2003). Long-term depression induced by sensory deprivation during cortical map plasticity in vivo. Nat. Neurosci. *6*, 291–299.

Antonini, A., and Stryker, M.P. (1993). Rapid remodeling of axonal arbors in the visual cortex. Science *260*, 1819–1821.

Atallah, B.V., Bruns, W., Carandini, M., and Scanziani, M. (2012). Parvalbumin-expressing interneurons linearly transform cortical responses to visual stimuli. Neuron *73*, 159–170.

Bender, K.J., Allen, C.B., Bender, V.A., and Feldman, D.E. (2006). Synaptic basis for whisker deprivation-induced synaptic depression in rat somatosensory cortex. J. Neurosci. *26*, 4155–4165.

Broser, P., Grinevich, V., Osten, P., Sakmann, B., and Wallace, D.J. (2008). Critical period plasticity of axonal arbors of layer 2/3 pyramidal neurons in rat somatosensory cortex: layer-specific reduction of projections into deprived cortical columns. Cereb. Cortex *18*, 1588–1603.

Bruno, R.M., Hahn, T.T., Wallace, D.J., de Kock, C.P., and Sakmann, B. (2009). Sensory experience alters specific branches of individual corticocortical axons during development. J. Neurosci. *29*, 3172–3181.

Buonomano, D.V., and Merzenich, M.M. (1998). Cortical plasticity: from synapses to maps. Annu. Rev. Neurosci. *21*, 149–186.

Buzsáki, G., and Wang, X.-J. (2012). Mechanisms of gamma oscillations. Annu. Rev. Neurosci. *35*, 203–225.

Cardin, J.A., Carlén, M., Meletis, K., Knoblich, U., Zhang, F., Deisseroth, K., Tsai, L.H., and Moore, C.I. (2009). Driving fast-spiking cells induces gamma rhythm and controls sensory responses. Nature *459*, 663–667.

Celikel, T., Szostak, V.A., and Feldman, D.E. (2004). Modulation of spike timing by sensory deprivation during induction of cortical map plasticity. Nat. Neurosci. *7*, 534–541.

Chattopadhyaya, B., Di Cristo, G., Higashiyama, H., Knott, G.W., Kuhlman, S.J., Welker, E., and Huang, Z.J. (2004). Experience and activity-dependent maturation of perisomatic GABAergic innervation in primary visual cortex during a postnatal critical period. J. Neurosci. *24*, 9598–9611.

Cheetham, C.E., Hammond, M.S., Edwards, C.E., and Finnerty, G.T. (2007). Sensory experience alters cortical connectivity and synaptic function site specifically. J. Neurosci. *27*, 3456–3465.

Cheetham, C.E., Hammond, M.S., McFarlane, R., and Finnerty, G.T. (2008). Altered sensory experience induces targeted rewiring of local excitatory connections in mature neocortex. J. Neurosci. *28*, 9249–9260.

Chittajallu, R., and Isaac, J.T. (2010). Emergence of cortical inhibition by coordinated sensory-driven plasticity at distinct synaptic loci. Nat. Neurosci. *13*, 1240–1248.

Chen, J.L., Lin, W.C., Cha, J.W., So, P.T., Kubota, Y., and Nedivi, E. (2011). Structural basis for the role of inhibition in facilitating adult brain plasticity. Nat. Neurosci. *14*, 587–594.

Clem, R.L., and Barth, A. (2006). Pathway-specific trafficking of native AMPARs by in vivo experience. Neuron *49*, 663–670.

Cruikshank, S.J., Urabe, H., Nurmikko, A.V., and Connors, B.W. (2010). Pathway-specific feedforward circuits between thalamus and neocortex revealed by selective optical stimulation of axons. Neuron *65*, 230–245.

Drew, P.J., and Feldman, D.E. (2009). Intrinsic signal imaging of deprivation-induced contraction of whisker representations in rat somatosensory cortex. Cereb. Cortex *19*, 331–348.

Feldman, D.E., and Brecht, M. (2005). Map plasticity in somatosensory cortex. Science *310*, 810–815.

Feldman, D.E. (2009). Synaptic mechanisms for plasticity in neocortex. Annu. Rev. Neurosci *32*, 33–55.

Feldmeyer, D., Lübke, J., Silver, R.A., and Sakmann, B. (2002). Synaptic connections between layer 4 spiny neurone-layer 2/3 pyramidal cell pairs in

juvenile rat barrel cortex: physiology and anatomy of interlaminar signalling within a cortical column. J. Physiol. *538*, 803–822.

Feldmeyer, D., Lübke, J., and Sakmann, B. (2006). Efficacy and connectivity of intracolumnar pairs of layer 2/3 pyramidal cells in the barrel cortex of juvenile rats. J. Physiol. *575*, 583–602.

Finnerty, G.T., Roberts, L.S., and Connors, B.W. (1999). Sensory experience modifies the short-term dynamics of neocortical synapses. Nature *400*, 367–371.

Fox, K. (2002). Anatomical pathways and molecular mechanisms for plasticity in the barrel cortex. Neuroscience *111*, 799–814.

Fries, P. (2009). Neuronal gamma-band synchronization as a fundamental process in cortical computation. Annu. Rev. Neurosci. *32*, 209–224.

Froemke, R.C., Merzenich, M.M., and Schreiner, C.E. (2007). A synaptic memory trace for cortical receptive field plasticity. Nature *450*, 425–429.

Gambino, F., and Holtmaat, A. (2012). Spike-timing-dependent potentiation of sensory surround in the somatosensory cortex is facilitated by deprivation-mediated disinhibition. Neuron *75*, 490–502.

Gandhi, S.P., Yanagawa, Y., and Stryker, M.P. (2008). Delayed plasticity of inhibitory neurons in developing visual cortex. Proc. Natl. Acad. Sci. USA *105*, 16797–16802.

Gentet, L.J. (2012). Functional diversity of supragranular GABAergic neurons in the barrel cortex. Front. Neural Circuits *6*, 52.

Glazewski, S., and Fox, K. (1996). Time course of experience-dependent synaptic potentiation and depression in barrel cortex of adolescent rats. J. Neurophysiol. *75*, 1714–1729.

Hardingham, N., Wright, N., Dachtler, J., and Fox, K. (2008). Sensory deprivation unmasks a PKA-dependent synaptic plasticity mechanism that operates in parallel with CaMKII. Neuron *60*, 861–874.

Helmstaedter, M., Sakmann, B., and Feldmeyer, D. (2009). Neuronal correlates of local, lateral, and translaminar inhibition with reference to cortical columns. Cereb. Cortex *19*, 926–937.

House, D.R., Elstrott, J., Koh, E., Chung, J., and Feldman, D.E. (2011). Parallel regulation of feedforward inhibition and excitation during whisker map plasticity. Neuron *72*, 819–831.

Jacob, V., Petreanu, L., Wright, N., Svoboda, K., and Fox, K. (2012). Regular spiking and intrinsic bursting pyramidal cells show orthogonal forms of experience-dependent plasticity in layer V of barrel cortex. Neuron *73*, 391–404.

Jadhav, S.P., Wolfe, J., and Feldman, D.E. (2009). Sparse temporal coding of elementary tactile features during active whisker sensation. Nat. Neurosci. *12*, 792–800.

Jiao, Y., Zhang, C., Yanagawa, Y., and Sun, Q.Q. (2006). Major effects of sensory experiences on the neocortical inhibitory circuits. J. Neurosci. *26*, 8691–8701.

Kapfer, C., Glickfeld, L.L., Atallah, B.V., and Scanziani, M. (2007). Supralinear increase of recurrent inhibition during sparse activity in the somatosensory cortex. Nat. Neurosci. *10*, 743–753.

Keck, T., Scheuss, V., Jacobsen, R.I., Wierenga, C.J., Eysel, U.T., Bonhoeffer, T., and Hübener, M. (2011). Loss of sensory input causes rapid structural changes of inhibitory neurons in adult mouse visual cortex. Neuron *71*, 869–882.

Lefort, S., Tomm, C., Floyd Sarria, J.C., and Petersen, C.C. (2009). The excitatory neuronal network of the C2 barrel column in mouse primary somatosensory cortex. Neuron *61*, 301–316.

Letzkus, J.J., Wolff, S.B., Meyer, E.M., Tovote, P., Courtin, J., Herry, C., and Lüthi, A. (2011). A disinhibitory microcircuit for associative fear learning in the auditory cortex. Nature *480*, 331–335.

Li, L., Bender, K.J., Drew, P.J., Jadhav, S.P., Sylwestrak, E., and Feldman, D.E. (2009). Endocannabinoid signaling is required for development and critical period plasticity of the whisker map in somatosensory cortex. Neuron *64*, 537–549.

Lu, J.T., Li, C.Y., Zhao, J.P., Poo, M.M., and Zhang, X.H. (2007). Spike-timing-dependent plasticity of neocortical excitatory synapses on inhibitory interneurons depends on target cell type. J. Neurosci. *27*, 9711–9720.

Maffei, A., and Turrigiano, G.G. (2008). Multiple modes of network homeostasis in visual cortical layer 2/3. J. Neurosci. *28*, 4377–4384.

Maffei, A., Nelson, S.B., and Turrigiano, G.G. (2004). Selective reconfiguration of layer 4 visual cortical circuitry by visual deprivation. Nat. Neurosci. *7*, 1353–1359.

Maffei, A., Nataraj, K., Nelson, S.B., and Turrigiano, G.G. (2006). Potentiation of cortical inhibition by visual deprivation. Nature *443*, 81–84.

Mateo, C., Avermann, M., Gentet, L.J., Zhang, F., Deisseroth, K., and Petersen, C.C. (2011). In vivo optogenetic stimulation of neocortical excitatory neurons drives brain-state-dependent inhibition. Curr. Biol. *21*, 1593–1602.

Marik, S.A., Yamahachi, H., McManus, J.N., Szabo, G., and Gilbert, C.D. (2010). Axonal dynamics of excitatory and inhibitory neurons in somatosensory cortex. PLoS Biol. *8*, e1000395.

Minlebaev, M., Colonnese, M., Tsintsadze, T., Sirota, A., and Khazipov, R. (2011). Early γ oscillations synchronize developing thalamus and cortex. Science *334*, 226–229.

Miyashita, T., Wintzer, M., Kurotani, T., Konishi, T., Ichinohe, N., and Rockland, K.S. (2010). Neurotrophin-3 is involved in the formation of apical dendritic bundles in cortical layer 2 of the rat. Cereb. Cortex *20*, 229–240.

Nagel, G., Brauner, M., Liewald, J.F., Adeishvili, N., Bamberg, E., and Gottschalk, A. (2005). Light activation of channelrhodopsin-2 in excitable cells of Caenorhabditis elegans triggers rapid behavioral responses. Curr. Biol. *15*, 2279–2284.

O'Connor, D.H., Peron, S.P., Huber, D., and Svoboda, K. (2010). Neural activity in barrel cortex underlying vibrissa-based object localization in mice. Neuron *67*, 1048–1061.

Paik, S.B., and Glaser, D.A. (2010). Synaptic plasticity controls sensory responses through frequency-dependent gamma oscillation resonance. PLoS Comput. Biol. *6*, e1000927.

Petreanu, L., Huber, D., Sobczyk, A., and Svoboda, K. (2007). Channelrhodopsin-2-assisted circuit mapping of long-range callosal projections. Nat. Neurosci. *10*, 663–668.

Reyes, A., Lujan, R., Rozov, A., Burnashev, N., Somogyi, P., and Sakmann, B. (1998). Target-cell-specific facilitation and depression in neocortical circuits. Nat. Neurosci. *1*, 279–285.

Sale, A., Berardi, N., Spolidoro, M., Baroncelli, L., and Maffei, L. (2010). GABAergic inhibition in visual cortical plasticity. Front. Cell Neurosci. *4*, 10.

Saito, T., and Nakatsuji, N. (2001). Efficient gene transfer into the embryonic mouse brain using in vivo electroporation. Dev. Biol. *240*, 237–246.

Schneider, T., and Neumaier, A. (2001). Algorithm 808: ARfit - a Matlab package for the estimation of parameters and eigenmodes of multivariate autoregressive models. ACM Trans. Math. Softw. *27*, 58–65.

Schummers, J., Mariño, J., and Sur, M. (2002). Synaptic integration by V1 neurons depends on location within the orientation map. Neuron *36*, 969–978.

Shepherd, G.M., Pologruto, T.A., and Svoboda, K. (2003). Circuit analysis of experience-dependent plasticity in the developing rat barrel cortex. Neuron *38*, 277–289.

Simons, D.J. (1978). Response properties of vibrissa units in rat SI somatosensory neocortex. J. Neurophysiol. *41*, 798–820.

Sirota, A., Montgomery, S., Fujisawa, S., Isomura, Y., Zugaro, M., and Buzsáki, G. (2008). Entrainment of neocortical neurons and gamma oscillations by the hippocampal theta rhythm. Neuron *60*, 683–697.

Sohal, V.S., Zhang, F., Yizhar, O., and Deisseroth, K. (2009). Parvalbumin neurons and gamma rhythms enhance cortical circuit performance. Nature *459*, 698–702.

Stern, E.A., Maravall, M., and Svoboda, K. (2001). Rapid development and plasticity of layer 2/3 maps in rat barrel cortex in vivo. Neuron *31*, 305–315.

Tabata, H., and Nakajima, K. (2001). Efficient in utero gene transfer system to the developing mouse brain using electroporation: visualization of neuronal migration in the developing cortex. Neuroscience *103*, 865–872.

Trachtenberg, J.T., and Stryker, M.P. (2001). Rapid anatomical plasticity of horizontal connections in the developing visual cortex. J. Neurosci. *21*, 3476–3482.

Turrigiano, G. (2012). Homeostatic synaptic plasticity: local and global mechanisms for stabilizing neuronal function. Cold Spring Harb. Perspect. Biol. *4*, a005736.

van Versendaal, D., Rajendran, R., Saiepour, M.H., Klooster, J., Smit-Rigter, L., Sommeijer, J.P., De Zeeuw, C.I., Hofer, S.B., Heimel, J.A., and Levelt, C.N. (2012). Elimination of inhibitory synapses is a major component of adult ocular dominance plasticity. Neuron *74*, 374–383.

Wang, X.J. (2010). Neurophysiological and computational principles of cortical rhythms in cognition. Physiol. Rev. *90*, 1195–1268.

Wen, J.A., and Barth, A.L. (2011). Input-specific critical periods for experience-dependent plasticity in layer 2/3 pyramidal neurons. J. Neurosci. *31*, 4456–4465.

Wilson, N.R., Runyan, C.A., Wang, F.L., and Sur, M. (2012). Division and subtraction by distinct cortical inhibitory networks in vivo. Nature *488*, 343–348.

Wimmer, V.C., Bruno, R.M., de Kock, C.P., Kuner, T., and Sakmann, B. (2010). Dimensions of a projection column and architecture of VPM and POm axons in rat vibrissal cortex. Cereb. Cortex *20*, 2265–2276.

Yamahachi, H., Marik, S.A., McManus, J.N., Denk, W., and Gilbert, C.D. (2009). Rapid axonal sprouting and pruning accompany functional reorganization in primary visual cortex. Neuron *64*, 719–729.

Yazaki-Sugiyama, Y., Kang, S., Câteau, H., Fukai, T., and Hensch, T.K. (2009). Bidirectional plasticity in fast-spiking GABA circuits by visual experience. Nature *462*, 218–221.